anomalies exhibit a steepness of the phase function ~5% greater than the surroundings. We produced an image of the phase ratio $f(39°)/f(86°)$ that is rather close to $f(44°)/f(96°)$, but using independent data acquired at red light $\lambda = 0.65$ μm with the Zeiss-600 telescope equipped with the LineScan camera (Fig. 3b). We confirm the same anomalous areas in Fig. 3a and b with similar contrast of ~5% relative to the adjacent mare regions. The anomalies are seen at larger phase angles too. Fig. 4 shows images of the phase ratio $f(71°)/f(108°)$. The relative contrast of the anomalous regions is somewhat smaller than in the previous cases, since at large phase angles the local slopes on resolved scales significantly contribute to the variations of image tones, which mask the details. We note that the anomalies are revealed on images of other phase ratios, though the choice of combinations of α_1 and α_2 influences the contrast of the anomalies.

To average this influence we utilized a parameter k using the function $\exp(-k\alpha)$ that is the best-fit regression for brightness images acquired with the 15-cm refractor (300D camera, red filter) at the phase angles 14.1°, 21.8°, 24.5°, 26.7°, 31.9°, 46.0°, 54.3°, 59.8°, 67.3°, and 73.1°. The least-squares method was used to fit the curve varying the parameter k. An image of k is shown in Fig. 5. Typical value of k for the anomalies is about 0.8, whereas, that of the surrounding mare areas reveal $k = 0.75$. Because of slightly different spatial resolutions of the brightness images used, the image of the parameter k shows an enhancement of high spatial frequencies: one can see weak dark halos around bright details. Overall the results concerning the Oceanus Procellarum anomalies found with the detectors of 300D, 350D, and CCD Sony ILX707 are confirmed using other wavelengths.

We examine areas of the Oceanus Procellarum anomalies with orbital images of higher resolution obtained with Lunar Orbiter IV and Apollo-16 cameras. The images acquired at low Sun reveal no apparent topography associated with the photometric anomalies. Fig. 6a–c presents, respectively, high-resolution Lunar Orbiter IV frame (for the anomaly 1) (http://astrogeology.usgs.gov/Projects/LunarOrbiterDigitization/) and Apollo frames AS16-M-2990 (for the anomaly 2) and AS16-M-2986 (for the anomaly 3) from the Apollo Image Archive at Arizona State University (http://apollo. sese.asu.edu/). The boundaries of the anomalies are shown in these figures.

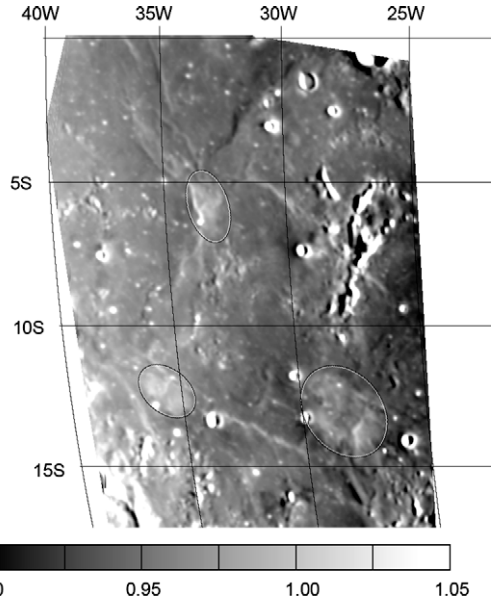

Fig. 4. Phase-ratio image $f(71°)/f(108°)$ at green light $\lambda = 0.53$ μm for the scene shown in Fig. 1.

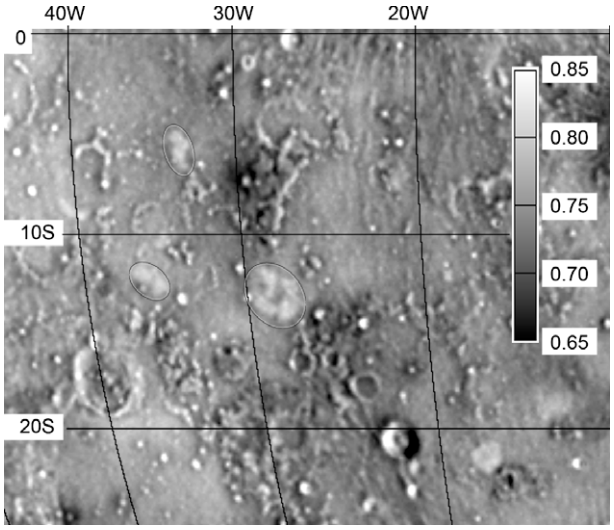

Fig. 5. The image shows a distribution of the parameter k of the function $\exp(-k\alpha)$ approximating phase dependences determined with brightness images acquired in red light $\lambda = 0.65$ μm at the phase angles 14.1°, 21.8°, 24.5°, 26.7°, 31.9°, 46.0°, 54.3°, 59.8°, 67.3°, 73.1°.

In addition, we searched for the anomalies on radar (70 and 3.8 cm) (Campbell and Ward, 2007; Zisk et al., 1974), magnetic (e.g., Halekas et al., 2001), and thermal inertia (Shorthill, 1973) maps and we were unable to detect the anomalies. Overall, these facts indicate that high slopes of phase curves are not due to the presence of large boulders and blocks scattered on the surface of the anomaly regions. We are reminded that the high phase-curve steepness of some proximal crater ejecta zones (the same kind of photometric anomaly) are certainly related to increased mesoscale roughness in these zones (Kreslavsky and Shkuratov, 2003), as they are clearly seen in the radar and thermal inertia maps. Obviously, the phenomenon considered here, in connection with the Oceanus Procellarum anomalies, is related to the delicate surface roughness at the very upper layer of the lunar regolith.

To consider possible differences in the surface composition and maturity degree we present in Figs. 7 and 8 distributions of the color ratios C_{RB}(0.60/0.47 μm) and C_{IR}(0.95/0.75 μm). The latter map was produced from Clementine data. Brighter shades in Figs. 7 and 8 denote greater values of these ratios. In a first approximation the parameter C_{IR} indicates areas of immature regolith; whereas, the ratio C_{RB} correlates with the TiO_2 content in mare soils (e.g., Charette et al., 1974; Blewett et al., 1997; Lucey et al., 1998; Shkuratov et al., 1999b, 2007a; Gillis et al., 2003; Gillis-Davis et al., 2006). All detected photometric anomalies have weak excesses in C_{RB}, which may be interpreted as there being little difference in composition of the surface material. Sites 1–3 exhibit lower values of C_{IR} ratio. Thus this may suggest a slightly lower regolith maturity of these sites. We note that the color and phase-ratio boundaries of the considered details often do not coincide.

The described anomalies can be easily found on polarimetric images at large phase angles (Shkuratov, 1981; Shkuratov and Opanasenko, 1992; Shkuratov et al., 2007b; Opanasenko et al., 2009a). On the other hand, we did not detect them as peculiarities with imaging polarimetry at small phase angles, mapping the parameters P_{min} and α_{inv} (Shkuratov et al., 2008).

Studying the polarimetric properties of the lunar surface is rather difficult. There is a close inverse correlation between albedo A and polarization degree P of light scattered by regolith-like media at large phase angles that is referred to as Umov's law. The correlation is approximately linear on a log–log scale: $\log P + a\log A = b$, and the correlation coefficient is up to 0.95. Hence, a direct mapping of